FIBRES & TEXTILES in Eastern Europe

sciendo

FIBRES & TEXTILES in Eastern Europe

Research Article • DOI: 10.2478/ftee-2022-0009 FTEE • 30(2) • 2022 • 68–74

Fabrication and Properties of Self-crimp Side-by-Side Bicomponent Filaments Composed of Polyethylene Terephthalates with Different Intrinsic Viscosity

Guodong Xiang[1], Hongjing Hua[1], Qingwen Gao[1], Jingwen Guo[1], Xuzhen Zhang[1], Xiuhua Wang[1]*

[1] *National Engineering Lab for Textile Fiber Materials and Processing Technology, Zhejiang Sci-Tech University, Hangzhou 310018, China*
* *Corresponding author. E-mail: wxiuhua@126.com*

Abstract
Self-crimp side-by-side bicomponent filaments (SBSBFs) were prepared via melt spinning using two kinds of polyethylene terephthalate (PET) with great disparity of intrinsic viscosity. The influence of the volume ratio on the surface morphology, crystallinity, crimping properties, mechanical properties and shrinkage properties of the bicomponent filaments was investigated using wide-angle X-ray diffraction, a differential scanning calorimetry (DSC), scanning electron microscope, etc. As the proportion of the low-viscosity component increases, the shrinkage in boiling water or hot air, as well as the shrinkage force and the sonic orientation factor of the bicomponent filaments decrease, and the DSC heating curves change from double peaks to a single peak. These phenomena should be ascribed to the high orientation and low crystallinity of the high-viscosity PET component and low orientation and high crystallinity of the low-viscosity PET component. Moreover, the crimp property of the bicomponent filament with a volume ratio of 50:50 is superior to those with other volume ratios.

Keywords
polyethylene terephthalate, self-crimp, side-by-side bicomponent filament, mechanical properties, shrinkage, crimp properties.

1. Introduction

Self-crimp bicomponent filaments have been widely applied in clothing and technical textiles. The characteristics of such filaments are that they can easily form three-dimensional curls like wool fibers after heating setting [1-2]. Self-crimp bicomponent filaments are usually made of two polymers arranged in a side-by-side or eccentric sheath-core manner [3-4], as shown in Figure 1. The crimps are generated from the shrinkage difference of two components, hence they have good stability. Side-by-side bicomponent filaments (SBSBFs) are produced from two polymers with similar chemical structures and a strong adhesive force between them to avoid interfacial peeling during drafting [5].

The most widely used self-crimp filaments on the market are SBSBFs made of polyethylene terephthalate (PET) and/or poly(trimethylene terephthalate) (PTT). Tae [6-7] studied the crimp properties of SBSBFs made of PTTs of different viscosities. Increasing the draw ratio caused a shrinkage difference between the two parts of the PTT and resulted in self-crimping of the fibers. The results indicated that the drawing ratio was the most critical variable in controlling the crimp contraction. Kan et al. [8] studied the crimp properties of PTT/PET SBSBFs with different component ratios. The crimpability of PET/PTT (50/50) filament was found superior to that of PET/PTT (40/60) or PET/PTT (60/40) filament. For PET/PTT, PET/PBT, and PET/cationic dyeable polyester filaments, optimum self-crimp properties were obtained for filament with a volume ratio of 50:50 and fineness of 8 dpf [9-10]. Liu et al. [11] investigated the elasticity of fabrics made of PTT/PET SBSBFs as weft yarn. They found that the larger the intrinsic viscosity difference between PTT and PET, the higher the elongation ratio of the corresponding PTT/PET bicomponent fabrics. The intrinsic viscosity difference caused the thermal shrinkage difference of PTT and PET in filaments, which eventually enhanced the crimp elasticity of the filaments and the elongation ratio of its corresponding fabrics. Jin [12] observed the cross-sections and longitudinal self-crimping configurations of various PTT/PET filaments via a microscope and calculated the crimp parameters, including helices pitches, crimp radii and crimp curvatures. The crimp curvature was found to increase with the increasing length ratio of the long axis to the short axis of the cross-section.

Commercial self-crimp products of DuPont T-400 (PET/PTT SBSBFs) were very popular in earlier years [9]. In recent years, improving the properties of PET/PTT filaments has aroused great interest [14,15]. Nevertheless, the

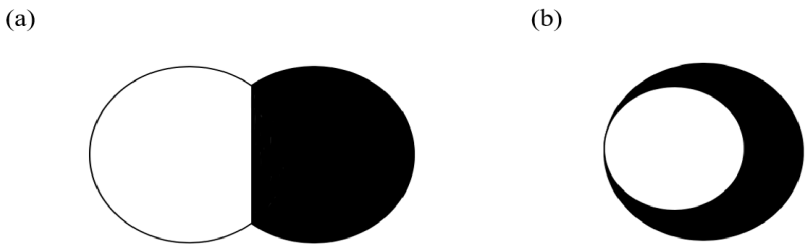


Fig. 1. Cross-sections of self-crimp filaments: (a) side-by-side, (b) eccentric sheath-core

Open Access. © 2022 Guodong Xiang et al., published by Sciendo. BY-NC-ND This work is licensed under the Creative Commons Attribution alone 3.0 License.

commercialisation and application of the filaments have been limited by the high price of PTT. Moreover, the dyeability of PET and PTT are quite different, which increases the cost and difficulty of dyeing [13]. PET with high viscosity (H-PET) and PET with low viscosity (L-PET) have similar dyeability and a remarkable difference in shrinkage, which provides an alternative choice to produce SBSBFs with a cost advantage. However, no report on H-PET/L-PET SBSBFs has been found so far.

In this paper, H-PET/L-PET filaments were prepared using two kinds of PET with great disparity of intrinsic viscosity. By designing a special spinneret, SBSBFs with different volume ratios were produced via melt spinning. This paper aimed to study the effect of volume ratios on the thermal properties, crystallization behaviours, mechanical properties, crimp properties and cross-sectional morphologies of the final filaments.

2. Experiment

2.1. Materials

PET pellets were supplied by Sinopec Shanghai Petrochemical Co. Ltd. (Shanghai, China). H-PET (M_v = 27163) pellets have an intrinsic viscosity of 0.908 dL/g and L-PET (M_v = 13186) pellets - 0.502 dL/g.

2.2. Preparation of H-PET/L-PET filaments

H-PET/L-PET SBSBFs were manufactured using a spinning-drawing machine (Huitong Co., Yangzhou, China). Specifications of the filaments are listed in Table 1.

The processing parameters are given in Table 2.

To display clearly the interface between the two components in the optical microscope images, a black masterbatch was added to the H-PET component. H-PET/H-PET (50/50) and L-PET/L-PET (50/50) filaments were produced at 325 ˚C and 276˚C, respectively.

Component	H- PET/ L- PET				
Specification	110 dtex /34f				
Volume Ratio	70:30	60:40	50:50	40:60	30:70

Table 1. Specifications of H-PET/L-PET SBSBFs

Items		Parameter
Temperature of extruder(˚C)	H-PET	292/325/325
	L-PET	272/277/276
Spinning manifold	Temperature (˚C)	305
GR1 (Godet roller 1)	Temperature (˚C)	85
	Speed (m/min)	2310
GR2 (Godet roller 2)	Temperature (˚C)	125
	Speed (m/min)	4310
WR (Winding roller)	Speed (m/min)	4200

Table 2. Spinning and drawing conditions

2.3. Characterisation

Morphologies of H-PET/L-PET SBSBFs, firstly frozen and cryofractured in liquid nitrogen, and then sputtered with a gold layer, were observed with a field emission scanning electron microscope (FESEM, JEOL Ltd., Japan). An optical microscope (Olympus Co., Japan) was also used to study the morphologies of H-PET/L-PET filaments. Physical images of the filaments were taken using a microscope (type XTL-25, Pudan Optical instrument Co., Ltd, Shanghai, China).

A rheology test was carried out using a capillary rheometer (Malvern Panalytical, UK). PET melt was tested flowing through a capillary with a diameter of 0.5mm and aspect ratio (L/D) of 16 at a given temperature and shear rate ranging from 200 to 6000 s^{-1}. Before the tests, the H-PET and L-PET pellets were dried in vacuum at 120˚C for 12 h.

Thermal properties of the PET pellets and bicomponent filaments were investigated using a differential scanning calorimeter (DSC, Mettler, Switzerland) in a nitrogen gas atmosphere with at a flow rate of 50mL/min. The temperature was raised from 25˚C to 290˚C at a heating rate of 10˚C/min and then kept at 290˚C for 5min. An X-ray powder diffractometer with a Cu target (Thermo Co., United States) was employed to investigate the crystallisation of the bicomponent filaments. All filaments were tested in a scanning angle range of 5 to 60° at a scanning speed of 3°/min. The sonic orientation of the bicomponent filaments was tested using a sonic orientation velocimeter (S.R.D. Scientific Instrument Co., Ltd, Shanghai, China) to determine the sound propagation time in filaments at a length of 20 cm or 40 cm, respectively. The orientation factor (f_s) was calculated according to the Equation 1:

$$f_s = 1\text{-}C_u^2/C^2 \quad (1)$$

Where C_u=1.35 km/s is the velocity of the acoustic wave passing through the filament [16], and C is the propagation velocity of the acoustic wave in the filaments.

The tensile strength and elongation at break of the filaments were tested on a single yarn strength machine (New Textile Testing Instruments and Equipment Co., Ltd, Changzhou, China) according to the GB/T 14344-2008 standard. Each sample was measured at a clamping distance of 500 mm, stretching speed of 500 mm/min, and pre-stress of 0.05 ± 0.005 cN/dtex. Every parameter was tested 5 times and then averaged. Shrinkage in boiling water was tested according to GB/T 6505-2008. Before being tested, all filaments were treated in boiling water at 100 ˚C for 30 min. A shrinkage-in-hot-air test was carried out using a thermal

shrinkage tester (Lenzing Instruments, Austria). The temperature was raised from 50 ˚C to 250 ˚C at a heating rate of 5 ˚C/min. Crimp properties of the filaments were tested after treatment in an oven at 160 ˚C for 30 min according to the GB/T 6506-2001 standard. Crimp properties including the crimp ratio, crimp modulus and crimp stability were calculated according to the Equations 2, 3, and 4 :

$$\text{Crimp ratio (\%)} = [(L_g - L_z)/L_g] \times 100\% \quad (2)$$

$$\text{Crimp modulus (\%)} = [(L_g - L_f)/L_g] \times 100\% \quad (3)$$

$$\text{Crimp stability (\%)} = [(L_g - L_b)/(L_g - L_z)] \times 100\% \quad (4)$$

Where L_g is the length of the fiber measured under a light load, L_z the length of the fiber measured under a heavy load, and L_b is the length of the fiber released from the heavy load, recovered after 10s, and then measured under a light load. The lengths are in mm.

3. Results and discussion

3.1. Melting behaviours of PET pellets

DSC curves of the H-PET and L-PET pellets are shown in Figure 2a. After eliminating the heat history at 300˚C, neither glass transition nor a cold crystallisation signal appears in the secondary heating curve of L-PET pellets. For H-PET pellets, the corresponding curve shows a glass transition at 79.7 ˚C and a cold crystallization peak at 155 ˚C. Both H-PET and L-PET have melting peaks around 254 ˚C. Their thermal crystallization peaks are 182 ˚C and 197 ˚C, respectively. L-PET is more susceptible to crystallisation than H-PET, which is similar to other studies [17].

The viscosities of L-PET and H-PET as functions of shear rates were tested to investigate the fluidity of the two raw polymers and are shown in Figure 2b. At a given shear rate, the viscosity of L-PET at 270 ˚C is lower than that of H-PET at 300˚C. The results indicate that the fluidity of L-PET at a lower testing temperature is better than that of H-PET at a higher testing temperature.

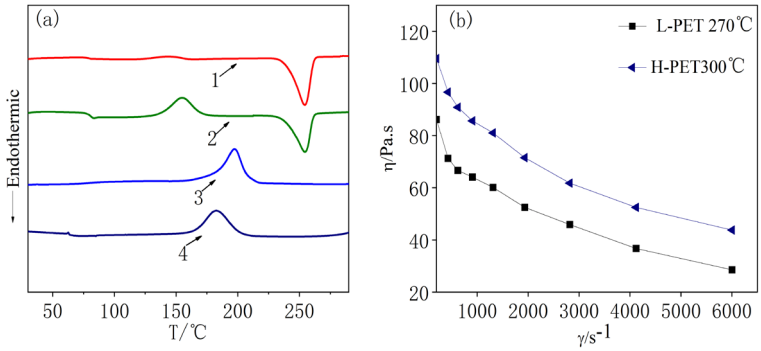


Fig. 2. Characteristics of H-PET and L-PET. (a) DSC curves (heating process of 1. L-PET and 2. H-PET, cooling process of 3. L-PET and 4. H-PET), (b) viscosity vs. shear rate curves

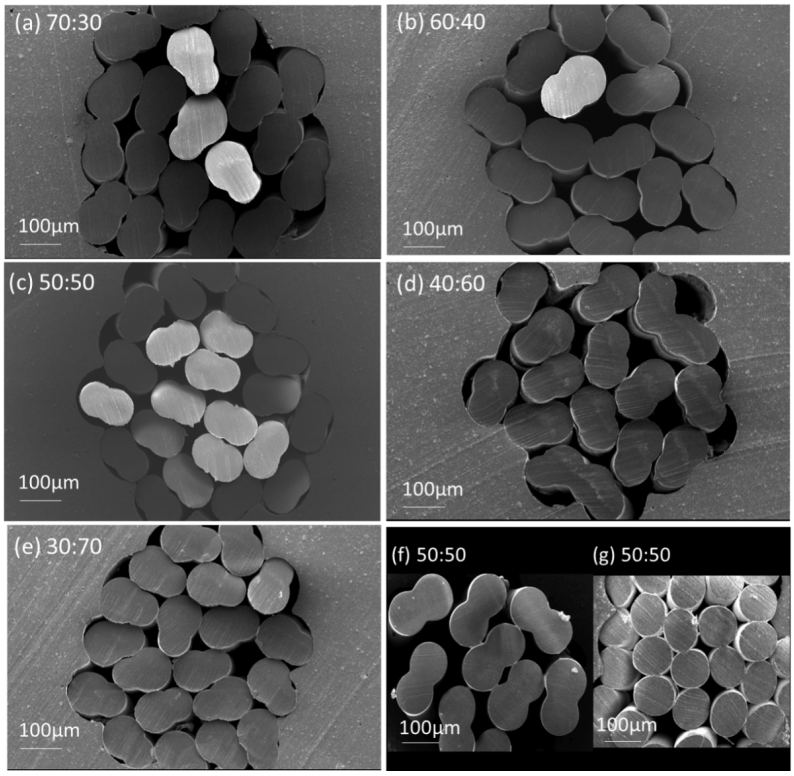


Fig. 3 .Cross-section SEM images of bicomponent filaments with various H-PET:L-PET ratios. (a) 70:30, (b) 60:40, (c) 50:50, (d) 40:60, (e) 30:70, (f) H-PET: H-PET 50:50, (g) L-PET: L-PET 50:50).

Cross-section morphologies of H-PET/L-PET SBSBFs of various volume ratios are shown in Figures 3a-e. Both H-PET/L-PET (30/70) and H-PET/L-PET (70/30) filaments have a pear shape cross-section morphology, while other filaments exhibit a peanut shape morphology. Figures 3f-g show the cross-sections of 50/50 pure H-PET and L-PET filaments. After flowing through the spinnerets, L-PET tends to form a circular cross-section due to its good fluidity (Figure 3g), while H-PET has a peanut shape due to its poor fluidity (Figure 3f).

Since the interface between two components cannot be seen in SEM images, optical microscope (OM) images were taken to investigate interfaces. Figure 4 shows that H-PET/L-PET (70/30) bicomponent filaments have straight interface lines. With increasing L-PET content, the straight interface lines of bicomponent filaments tend to curve. The low-viscosity component always tends to encapsulate

the high-viscosity component, which is consistent with the above-mentioned single component filaments [12].

3.2. Orientation

Figure 5a shows the sonic orientation factors of H-PET/L-PET SBSBFs. The orientation factor of H-PET/L-PET (70/30) bicomponent filaments is 77.5. As the proportion of H-PET decreases, the sonic orientation factor decreases gradually. This is because the H-PET component in the filaments will bear stronger tensile stress than the L-PET component during the spinning process. Molecular chains of H-PET are arranged preferentially along the direction of the external force, leading to a higher orientation of H-PET [18].

3.3. Crystallinity

Figure 5b shows the wide-angle X-ray diffraction patterns of bicomponent filaments. All filaments exhibit diffraction peaks at 17.5°, 22.44° and 25.48°, which correspond to the crystal planes of (010), (110), and (100) in the triclinic system of PET crystal, respectively [19-20]. The locations of diffraction peaks are similar for all filaments, indicating their similarity of crystal form.

Figure 5c shows DSC first heating curves of the filaments, the corresponding paraments of which are summarised in Table 3. The heating curve of H-PET/L-PET (70/30) bicomponent filaments shows double melting endothermal peaks, the main melting peak, located around 259 ˚C, and the neck melting peak, located around 252 ˚C. With a decreasing H-PET content, the neck melting peak moves toward high temperature, leading to a single melting endothermal peak.

This indicates that the H-PET component of the bicomponent filaments contributes to the neck melting peak and the L-PET component to the main melting peak. This is because H-PET has a higher molecular weight, hence it is more difficult to crystallise than L-PET [21-23]. As a result, the L-PET component has a low-orientation, high crystallisation supramolecular structure, while the H-PET component has a high orientation and low crystallisation structure in the bicomponent filaments.

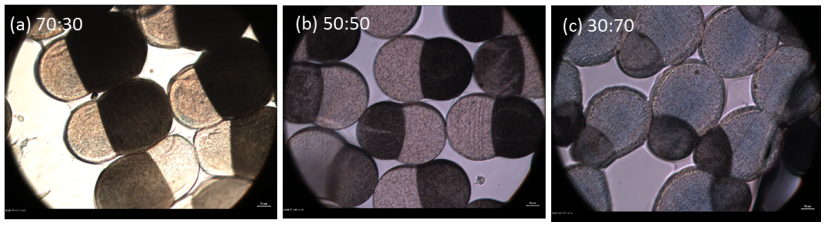


Fig. 4. OM images of cross-sections (500×) of coloured H-PET/L-PET SBSBFs with various H-PET:L-PET ratios, where the black component is the high-viscosity component. (a) 70:30, (b) 50:50, (c) 30:70)

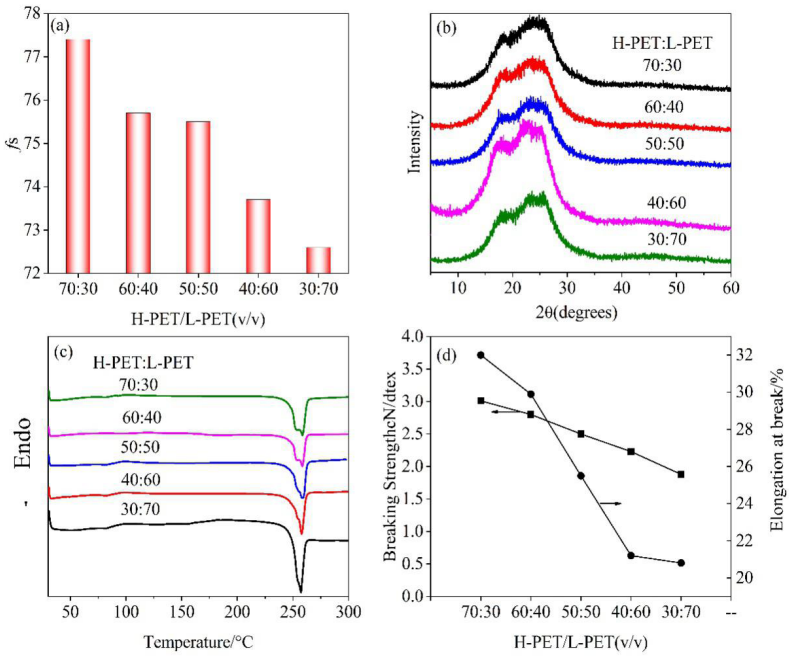


Fig. 5. Characteristics of H-PET/L-PET SBSBFs. (a) sonic orientation factor, (b) wide angle X-ray diffraction patterns, (c) DSC first heating curves, (d) mechanical properties

H-PET/L-PET	Neck melting peak/°C	Main melting peak/°C
70:30	252	259
60:40	253	358
50:50	256	258
40:60	255	258
30:70	257	257

Table 3. Melt temperatures of H-PET/L-PET SBSBFs

3.4. Mechanical properties

Figure 5d shows the mechanical properties of H-PET/L-PET filaments. The tensile strength and elongation at break of H-PET/L-PET (70/30) are 3.01 cN/dtex and 32%, respectively. As the proportion of the H-PET component decreases, both the breaking strength and elongation at break of H-PET/L-PET (30/70) decrease to 1.88 cN/dtex and 20.8% . The decrease in breaking strength attributed to less H-PET is related to a common rule that polymer with higher molecular weight often shows better mechanical properties

than those with lower molecular weight. With the increasing of the H-PET component, the breaking strength and elongation at break of the bicomponent filaments also increased. This is because the tensile strength and elongation of the filament are mainly determined by its weak part, that is, by the component with low elongation. At the same time, since the high-viscosity component is a part of the high strength and low elongation, as the high-viscosity component decreased, the strength of the bicomponent filaments decreased, along with the elongation at break synchronously [23-25].

3.5. Shrinkage

Figure 6 shows the shrinkage in boiling water of bicomponent filaments. With a decrease in H-PET content from 70% to 30%, the shrinkage of filaments gradually decreases. The data indicate that H-PET exhibits a greater shrinkage than L-PET. The occurrence of shrinkage is a result of the de-orientation of oriented molecules or segments in amorphous regions [26-27]. More of the H-PET component contributes to higher shrinkage since the H-PET component has a high orientation and low crystallisation structure in bicomponent filaments.

Figure 7 shows OM images of bicomponent filaments. After being heat treated in boiling water, the filaments show a curved morphology, with the inner side being observed as H-PET, while the outer side as L-PET, which indicates that the H-PET component is more sensitive in heat-shrinking than the L-PET component.

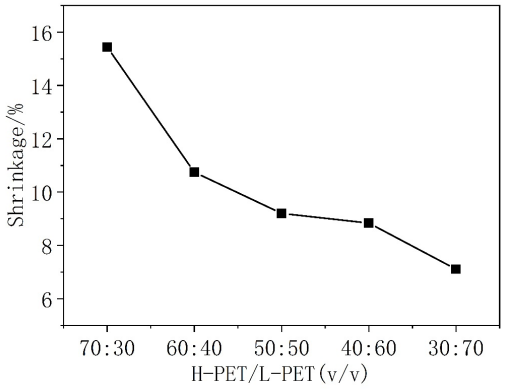


Fig. 6. Boiling water shrinkage of H- PET/L-PET SBSBFs

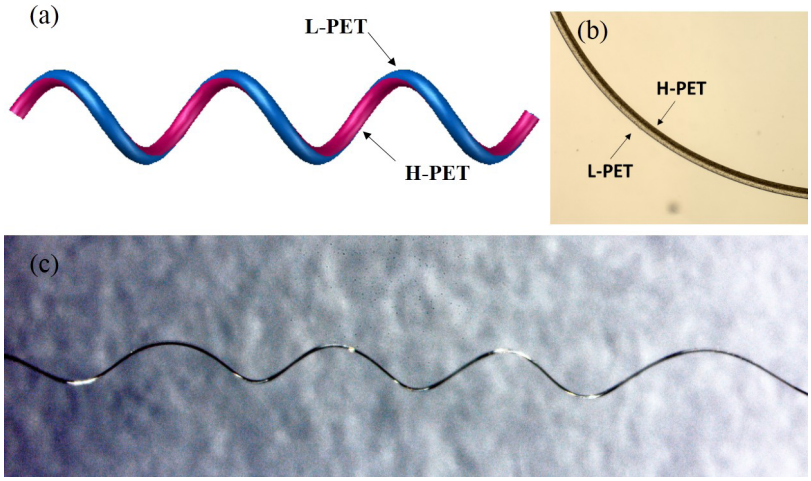


Fig. 7. Morphology of crimps of H-PET/L-PET SBSBFs. (a) model image, (b) OM image (500×), (c) physical image (25×)

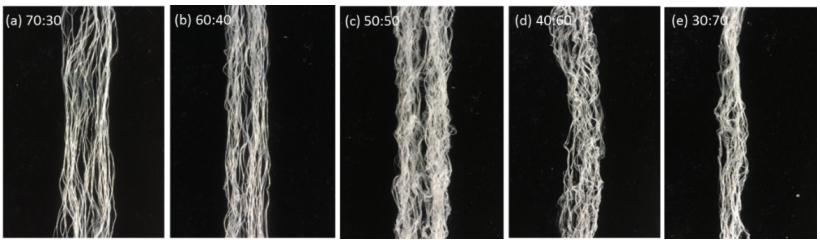


Fig. 8. Images of curved H-PET/L-PET SBSBFs after being treated in boiling water with various H-PET:L-PET ratios. (a) 70:30, (b) 60:40, (c) 50:50, (d) 40:60, (e) 30:70)

3.6. Crimp properties

All filaments exhibit a three-dimensional spiral shape after being treated in boiling water (Figure 8). H-PET/L-PET (50/50) filament (Figure 8c) clearly exhibits more obvious crimp behaviour than other filaments. This should be attributed to the equal content of the two components, which contributes to the straight-like interface between the two components and the crimp potential energy of the filaments when the two components have shrunk [15].

Figure 9 shows the crimp properties of H-PET/L-PET filaments. The crimp ratio of the H-PET/L-PET (50/50) filaments is 22.6 %, corresponding a crimp modulus and crimp stability of 7.2 % and 32.9 %, respectively. These crimp parameters are higher than those of filaments with other ratios, indicating that the crimp properties of H-PET/L-PET (50/50) filaments are the best among all the filaments prepared. According to Denton's theory [9], the crimp ratio resulting from the shrinkage difference is more affected by the ratio than by the elastic modulus of the two polymers.

4. Conclusions

In this paper, H-PET/L-PET SBSBFs were melt spun using two kinds of PET

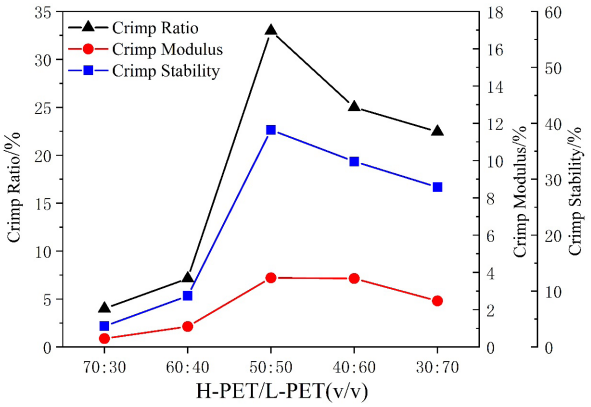


Fig. 9. Crimp ratio, crimp moduli and crimp stability of H-PET/L-PET SBSBFs

pellets with great disparity in molecular weight, indirectly testified by intrinsic viscosities of 0.908 dL/g and 0.502 dL/g. The similar dying property and remarkable shrinkage difference between H-PET and L-PET give H-PET/L-PET SBSBFs a lower cost and better dyeability as compared to traditional PET/PTT SBSBFs. Some conclusions are given below:

1. As the H-PET content decreases from 70% to 30%, the cross-sections of SBSBFs change from a pear shape to a peanut shape, and interface lines between the H-PET component and L-PET component in cross-sections change from being straight to being curved.
2. The sonic orientation factors of H-PET/L-PET SBSBFs decrease and melting peaks in DSC curves transform from double melting peaks to a single peak with an increasing L-PET content. The crystallinity of the L-PET component is higher than that of H-PET, while the orientation of L-PET is lower than that of H-PET.
3. Boiling water shrinkage, hot air shrinkage and the shrinkage force decrease with a decrease in H-PET content from 70% to 30%. Based on the crimp morphologies of H-PET/L-PET filaments, the H-PET component locates itself on the inner side of SBSBFs. The H-PET/L-PET (50/50) filament shows the best crimp properties among all the filaments.

Acknowledgements

This work was supported by China National Textile and Apparel Council Science and Technology Guiding Project (No. 2017002), China Postdoctoral Science Foundation (No. 2018M630691).

References

1. Xiao H, Shi MW, Liu LL. The Crystallinity and Orientation Structure and Crimp Properties of PET/PTT Bicomponent Filament. *Advanced Materials Research* 2013; 627(1): 110-116.
2. Chen SH, Wang SY. Effect of Thermal Stimuli on Physical Behaviors of PET/PTT Bicomponent Filament. *Advanced Materials Research* 2010; 129-131: 280-284.
3. Yang ZL, Wang FM. Dyeing and finishing performance of different PTT/PET bi-component filament fabrics. *Indian Journal of Fibre & Textile Research* 2016; 41(4): 411-417.
4. Chen SH, Wang SY. Tensile and Fracture Behaviors of PET/PTT Side-Side Bicomponent Filament. *International Journal of Polymer Analysis and Characterization* 2010; 15(3): 147-154.
5. Fang Y, Wang CH, Liang HF, Bao LL et al. Theoretical and experimental study on the crimp mechanism of bi-component filament. *Advanced Materials Research* 2012; 476-478(0): 2209-2212.
6. Oh TH. Effects of Spinning and Drawing Conditions on the Crimp Contraction of Side-by-Side Poly(trimethylene terephthalate) Bicomponent Fibers. *Journal of Applied Polymer Science* 2010; 102(2): 1322-1327.
7. Oh TH. Melt Spinning and Drawing Process of PET Side-by-Side Bicomponent Fibers. *Journal of Applied Polymer Science* 2006; 101(3): 1362-1367.
8. Lai K, Chen MY, Sun RJ et al. Study on the Crimp Property of PTT/PET Bicomponent Filament. *Advanced Materials Research* 2013; 781-784(0): 2680-2684.
9. Rwei SP, Lin YT, Su YY. Study of Self-Crimp Polyester Fibers. *Polymer Engineering and Science* 2005; 45(6): 838–845.
10. Dention MJ. The Crimp Curvature of Bicomponent Fibers. *Journal of the Textile Institute* 1982; 73(6): 253-263.
11. Liu XS, Jiao SY, Wang FM. Configuring the spinning technology of PTT/PET bicomponent filaments according to fabric elasticity. *Textile Research Journal* 2013; 83(5): 487-498.
12. Luo J ,Xu GB, Wang FM. External Configuration and Crimp Parameters of PTT (Polytrimethylene terephthalate)/PET (Polyethylene terephthalate) Conjugated Fiber. *Fibers and Polymers* 2009; 10(4):508-512.
13. Chuah HH. Orientation and Structure Development in Poly(trimethylene terephthalate) Tensile Drawing. *Macromolecules* 2001; 34(20): 6985-6993.
14. Guo J, Zheng N,Chen YT. Study on Influence of Crimping Performance of PET/PTT Self-Crimp Yarn Treated with Moist Heat. *Advanced Materials Research* 2011; 287-290(0): 2547-2551.
15. Chen SH ,Wang SY. Latent-Crimp Behavior of PET/PTT Elastomultiester and a Concise Interpretation. *Journal of Macromolecular Science*, Part B: Physics. 2011; 50(7): 1447-1459.
16. Jiang ZH, Guo ZG , Zhang ZQ. Preparation and properties of bottle-

recycled polyethylene terephthalate (PET) filaments. *Textil Research Journal* 2018; 89(7): 1207-1214.

17. Ayad E, Cayla AL, Rault F et al. Influence of Rheological and Thermal Properties of Polymers During Melt Spinning on Bicomponent Fiber Morphology. *Journal of Materials Engineering and Performance* 2016; 25(8): 3296-3302.
18. Petraccone V, Rosa CD, Guerra G et al. On the Double Peak Shape of Melting Endotherms of Isothermally Crystallized Isotactic Polypropylene Samples. *Die Makromolekulare Chemie Rapid Communications* 1984; 5(10): 631.
19. Wang Y, Sun YM, Zhu ZY et al. XRD Study of PET Irradiated by 1.158 GeV Fe Ions. IMP and *GIRFL Annual Report* 2002; (1): 63.
20. Hu JC, Yang D, Chen P et al. Studies on The Crystallinity of PET by WAXD. *Acta Polymerica Sinica* 1990; (3): 283.
21. Ren MQ, Zhang ZY, Wu SZ et al. Uniaxial Orientation and Crystallization Behavior of Amorphous Poly (ethylene terephthalate) Fibers. *Journal of Polymer Research* 2006; 13(1): 9-15.
22. Mehdi Z, Mojtaba S. Isothermal Crystallization Kinetics of Poly(Ethylene Terephthalate)S of Different Molecular Weights. *Journal of the Iranian Chemical Society* 2013; 10(1): 77-84.
23. Zhu PP, Ma DZ. Study on the Double Cold Crystallization Peaks of Poly (Ethylene Terephthalate) (PET): 2. Samples Isothermally Crystallized At High Temperature. *European Polymer Journal* 1999; 35(4): 739-742.
24. Xiao H, Shi MW, Liu LL et al. The Structures and Properties of PET (Polyethylene Terephthalate) /PTT (Polytrimethylene Terephthalate) Self-Crimp Filament at Different Temperatures. *Advanced Materials Research* 2011; 332-334(0): 239-245.
25. Wu AH, Xu GP, Luo GH et al. Study of the Mechanical Properties and Releasing Anion Capacity of Anionic Functional PET Fiber. *Applied Mechanics and Material* 2013; 423-426(0): 322-325.
26. Zhang X, Tian XY, Yao XY et al. Isothermal and Non-Isothermal Shrinkage Behaviors of Highly Oriented PET Yarns. *Fibers and Polymers* 2008; 9(3): 360-364.
27. Rim PB, Nelson CJ. Properties of PET Fibers with High Modulus and Low Shrinkage (HMLS). I. Yarn Properties and Morphology. *Applied Polymer. Sci.* 2010; 42(7): 1807-1813.